Supplementary Information

Highly pixelated, untethered tactile interfaces for an ultra-flexible on-skin telehaptic system

Hanbit Jin[1]*, Yunjeong Kim[1]*, Wooseup Youm[1], Yulim Min[1,2], Saerom Seo[1], Chaehyun Lim[1], Chan-Hwa Hong[1], Seyoung Kwon[3], Gyeongseok Park[3], Steve Park[3], Hye Jin Kim[1,2†]

[1] Electronics and Telecommunications Research Institute (ETRI), Daejeon, Korea

[2] Korea University of Science and Technology (UST), Daejeon, Korea

[3] Korea Advanced Institute of Science and Technology (KAIST), Daejeon, Korea

[*] These authors contributed equally to this work

Corresponding Author

† Hye Jin Kim, E-mail: nolawara@etri.re.kr

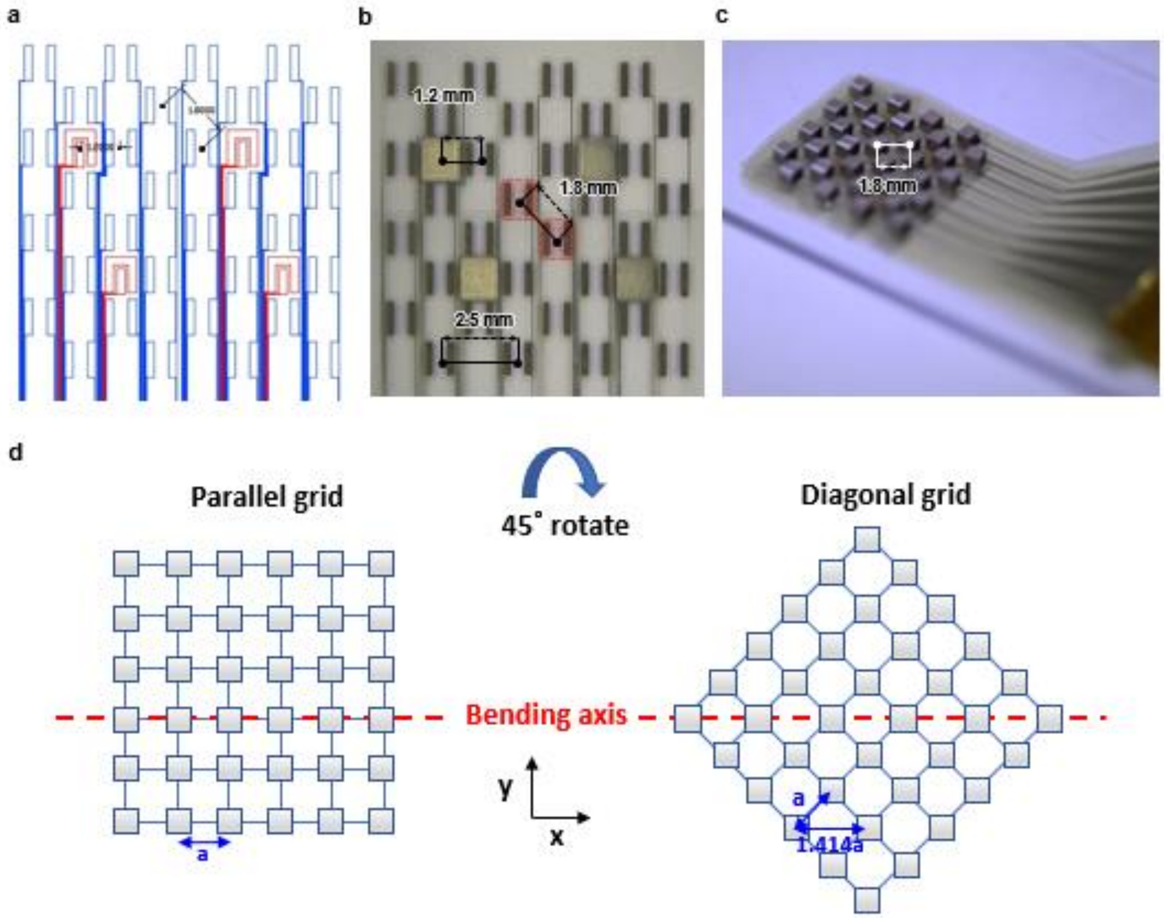

Supplementary Figure 1. Dimension of tactile sensor and actuator array. **a**. schematic of ultra-flexible substrate electrode patterns. Ultra-flexible substrate has 1.8 mm diagonal pitch resolution with chessboard pattern. **b**. image of ultra-flexible bimodal tactile sensor with dimension. **c**. image of ultra-flexible tactile actuator on slide glass with dimension. **d**. schematic of parallel and diagonal grid arrangements that have same spatial resolution (a = minimum distance to adjacent pixel)

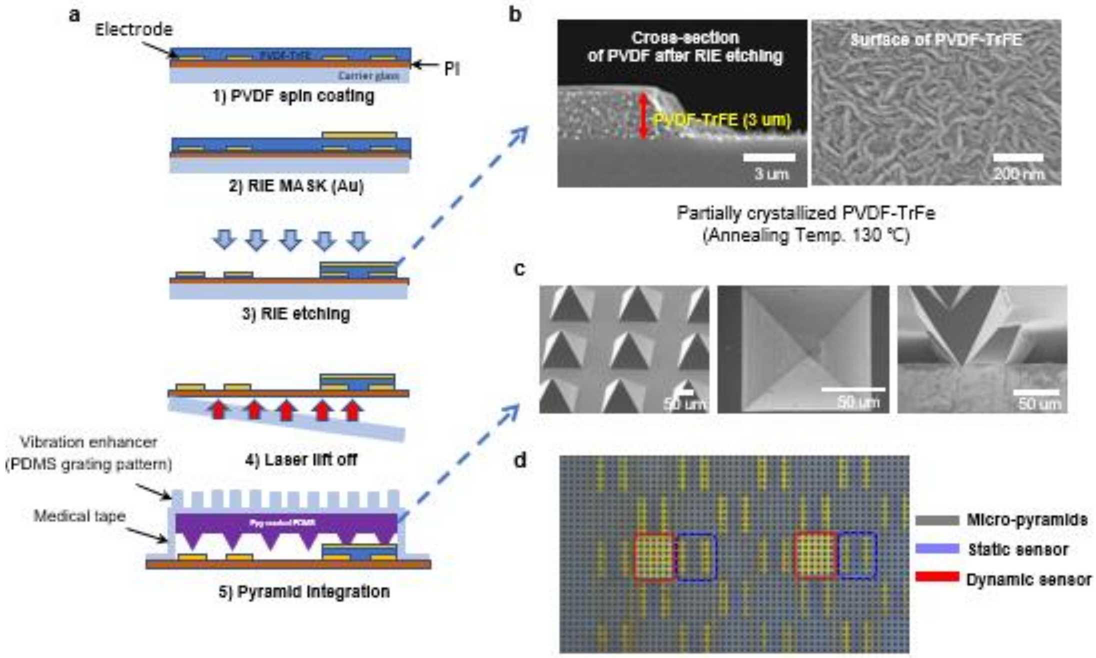

Supplementary Figure 2. Fabrication of the ultra-flexible bimodal sensor array. **a**, schematic of fabrication process flow. Spin coating, e-beam deposition, RIE process is compatible because the PI substrate is fabricated on the carrier glass. Finally, ultra-flexible sensor is peeled off by the laser lift-off process. **b**, SEM image of cross-section of PVDF-TrFE after RIE etching (left), **c**, SEM image of PDMS micro-pyramids, tilted view, top view, side view under pressure. **d**, optical microscopic image of bimodal sensor array after integration of micro-pyramids on static and dynamic sensor layer

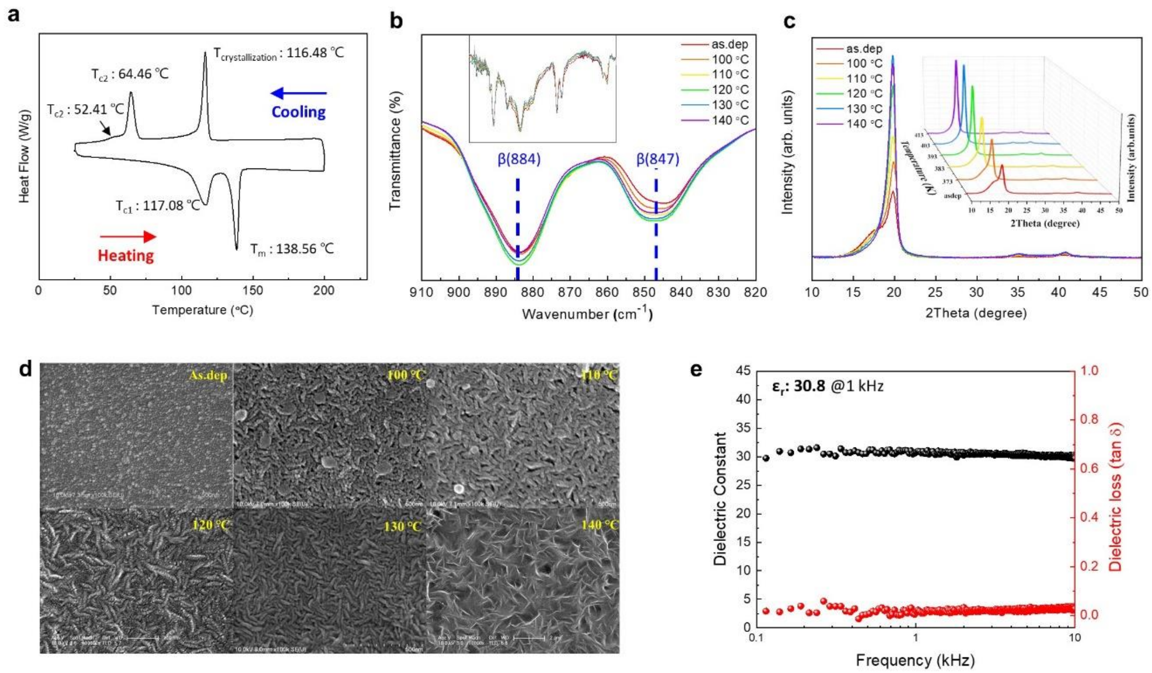

Supplementary Figure 3. Characteristics of PVDF-TrFE dynamic pressure sensor. **a**, differential scanning calorimetry of PVDF-TrFE. **b**, FT-IR spectra, **c**, XRD patterns, and **d**, FE-SEM images of PVDF-TrFE thin films treated at different annealing temperatures (as.dep, 100, 110, 120, 130, and 140 °C). **e**, dielectric constant and dielectric loss of thin films annealed at 130 °C (εr: 30.8 @ 1 kHz).

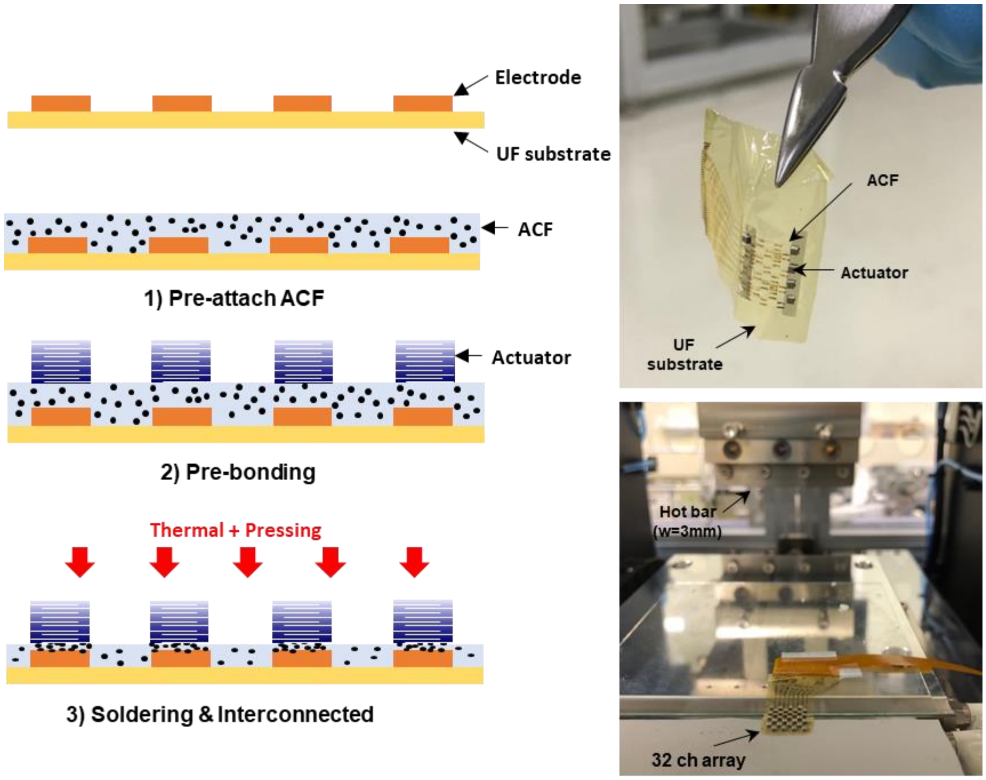

Supplementary Figure 4. Thermo-compression bonding process of ultra-flexible actuator array. Anisotropic conductive film (ACF) bonding has been used for establishing electrical contact between ultra-flexible substrate and miniaturized piezoelectric actuator.

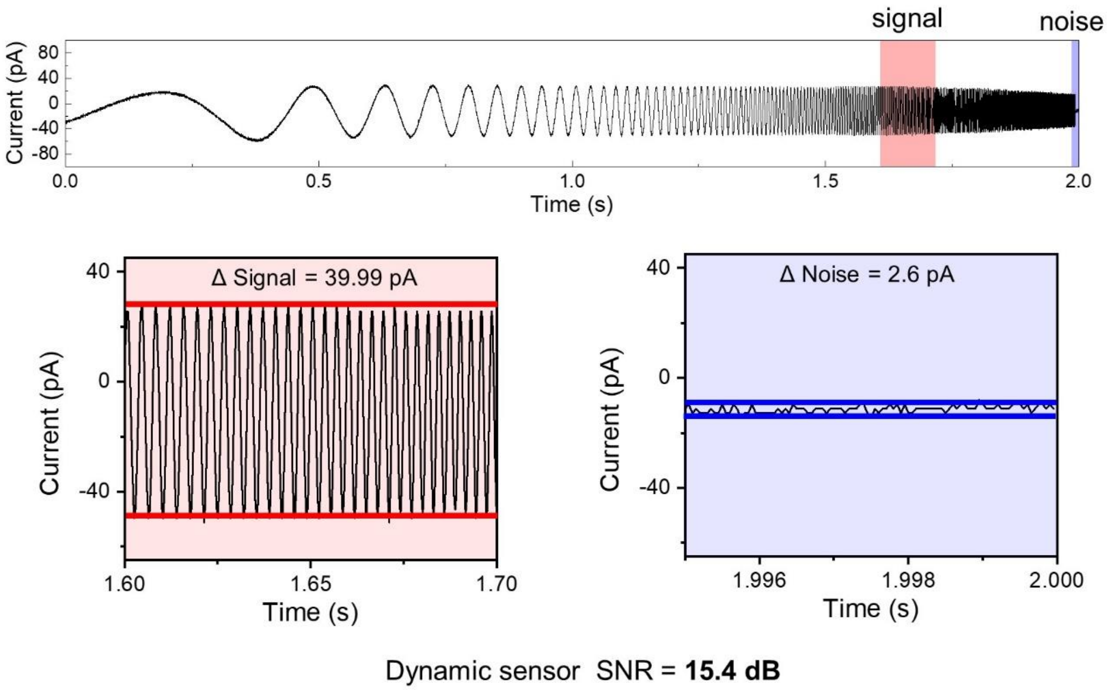

Supplementary Figure 5. Dynamic sensor characteristics, SNR of dynamic pressure sensor. Sine wave sweep signal (from 1 Hz to 1 kHz) was applied to the sensor and signal-to-noise ratio was calculated from signal and noise from base line.

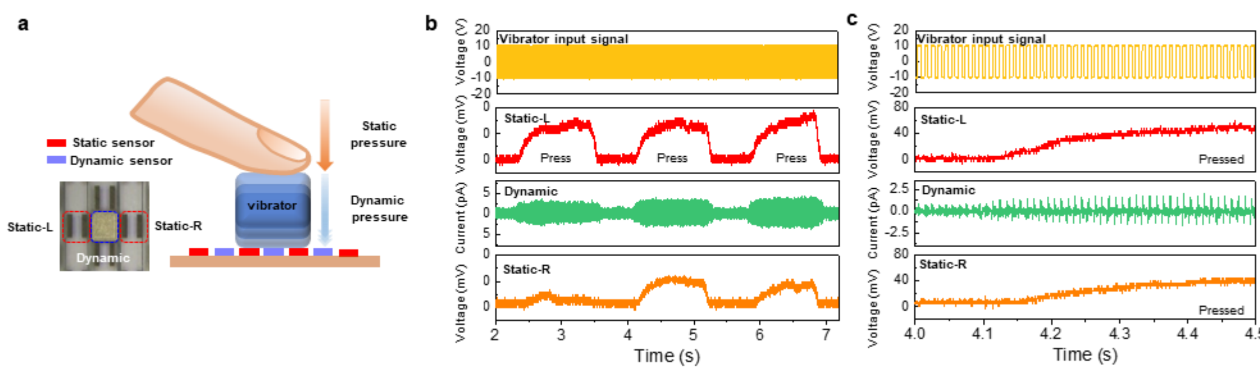

Supplementary Figure 6. a, Schematic of simultaneous monitoring of static and dynamic complex pressure by using UFB tactile sensor array. **b**, Selective detection of static/dynamic pressure by UFB tactile sensor array. **c**, Magnified plot of static and dynamic sensor signals.

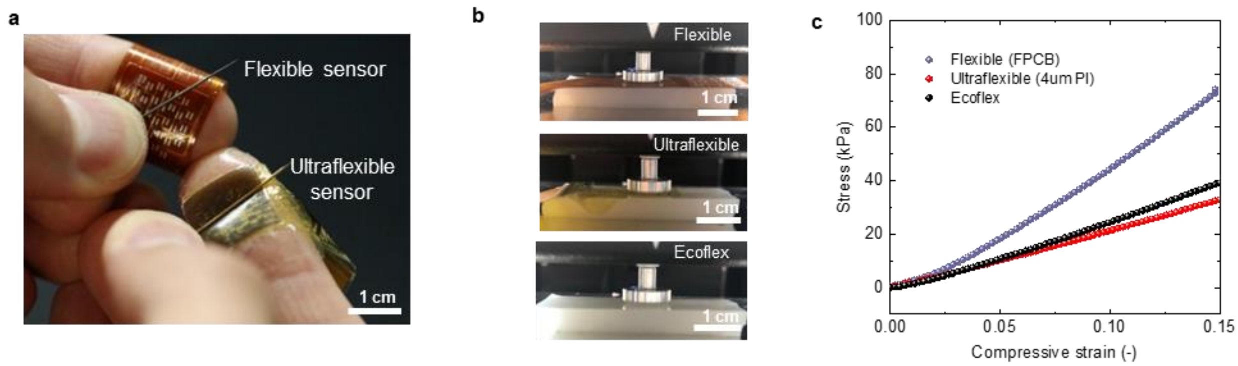

Supplementary Figure 7. a, Image of surface deformation while the attached UFB tactile sensor is pressed by a needle. **b**, Images of the mechanical compliance/stiffness test setup. **c**, Strain-stress curve of flexible substrate and ultra-flexible compressive strain. Conventional flexible substrate shows 2 times higher modulus than the UFB sensor.

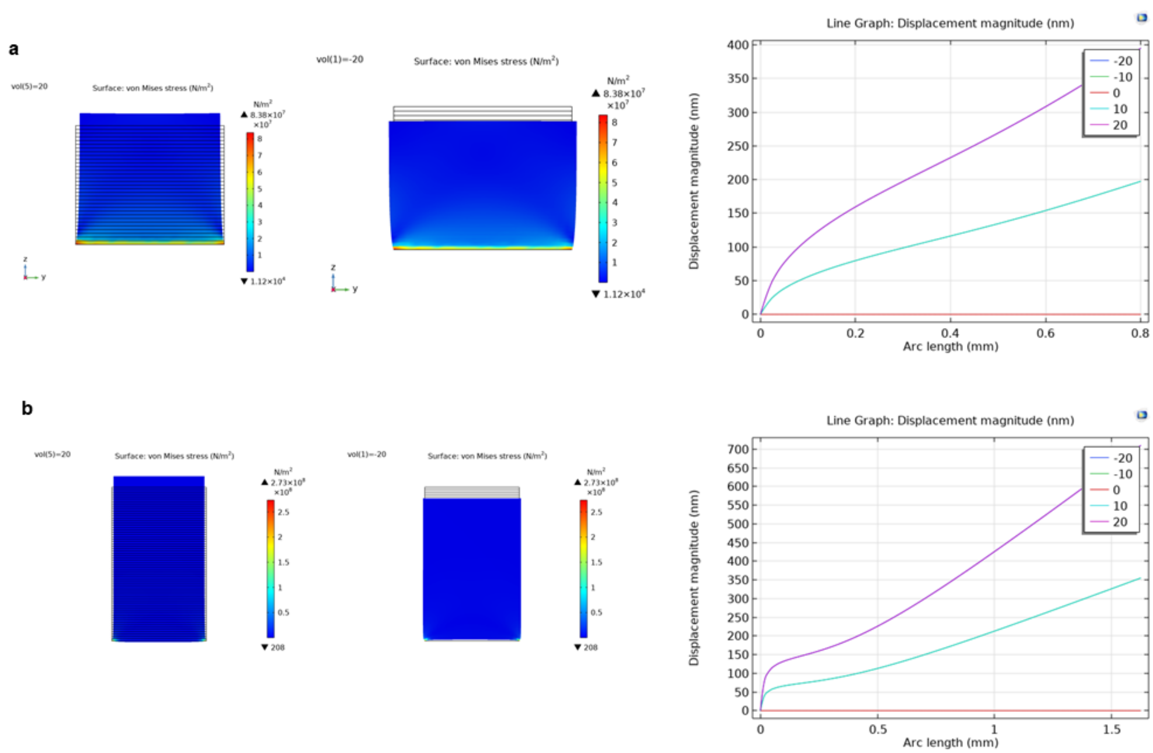

Supplementary Figure 8. Improvement of output performance by increasing stacked layers has been analysed by finite element analysis (FEA). **a**. stress distribution (left) and displacement (right) of multi-layered actuators that have 32 layers and **b**. 64 layers. Displacement has been significantly increased by doubling the number of stacked layers.

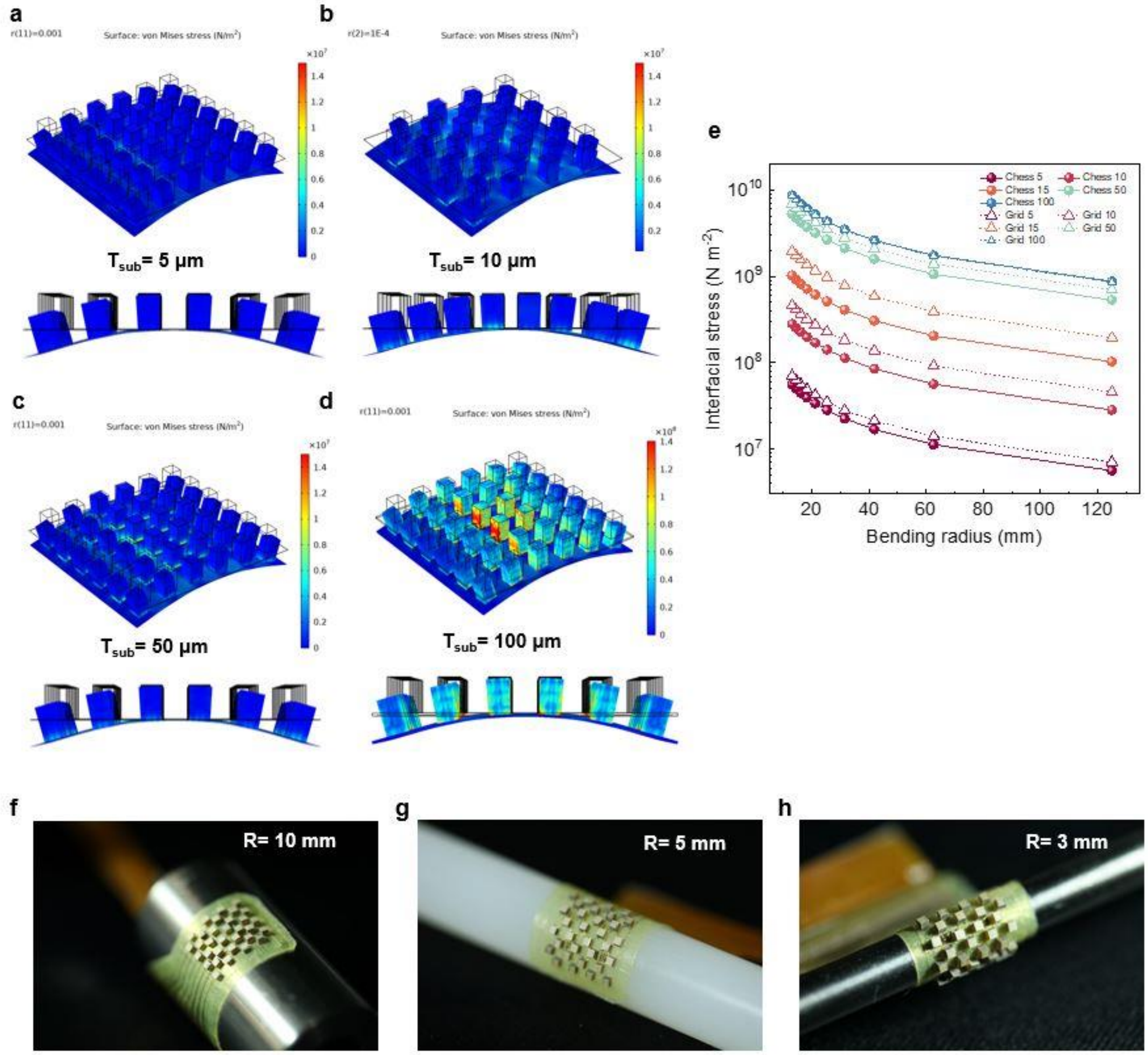

Supplementary Figure 9. FEM simulation of stress distribution in square grid pattern flexible actuator arrays that have various substrate thickness during bending and images of bending test. **a**, stress distribution on 5 μm-thick substrate, **b**, 10 μm-thick substrate, **c**, 50 μm-thick substrate, **d**, 100 μm-thick substrate, **e**, interfacial stress on various thickness of substrates during bending. Solid line is stress of chessboard arrangement and dashed line is stress of grid arrangement. Bending test of ultra-flexible actuator array with chess pattern at **f**, 10 mm, **g**, 5 mm and **h**, 3 mm bending radius.

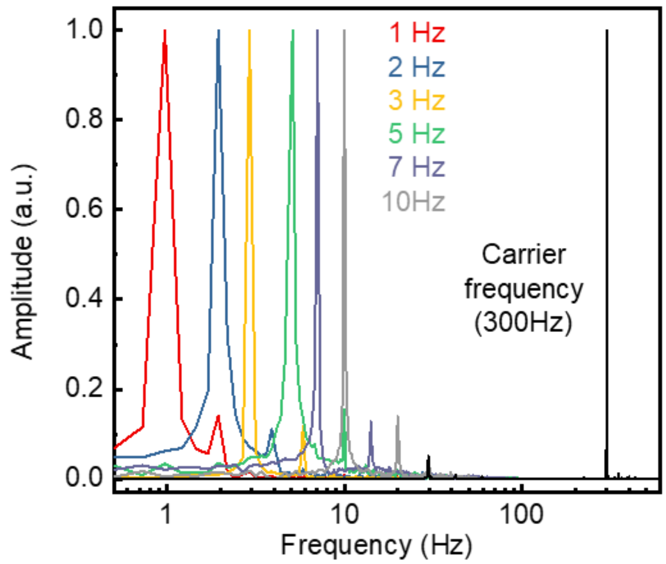

Supplementary Fig. 10. FFT analysis of modulated signals for imparting the sensation of static pressure

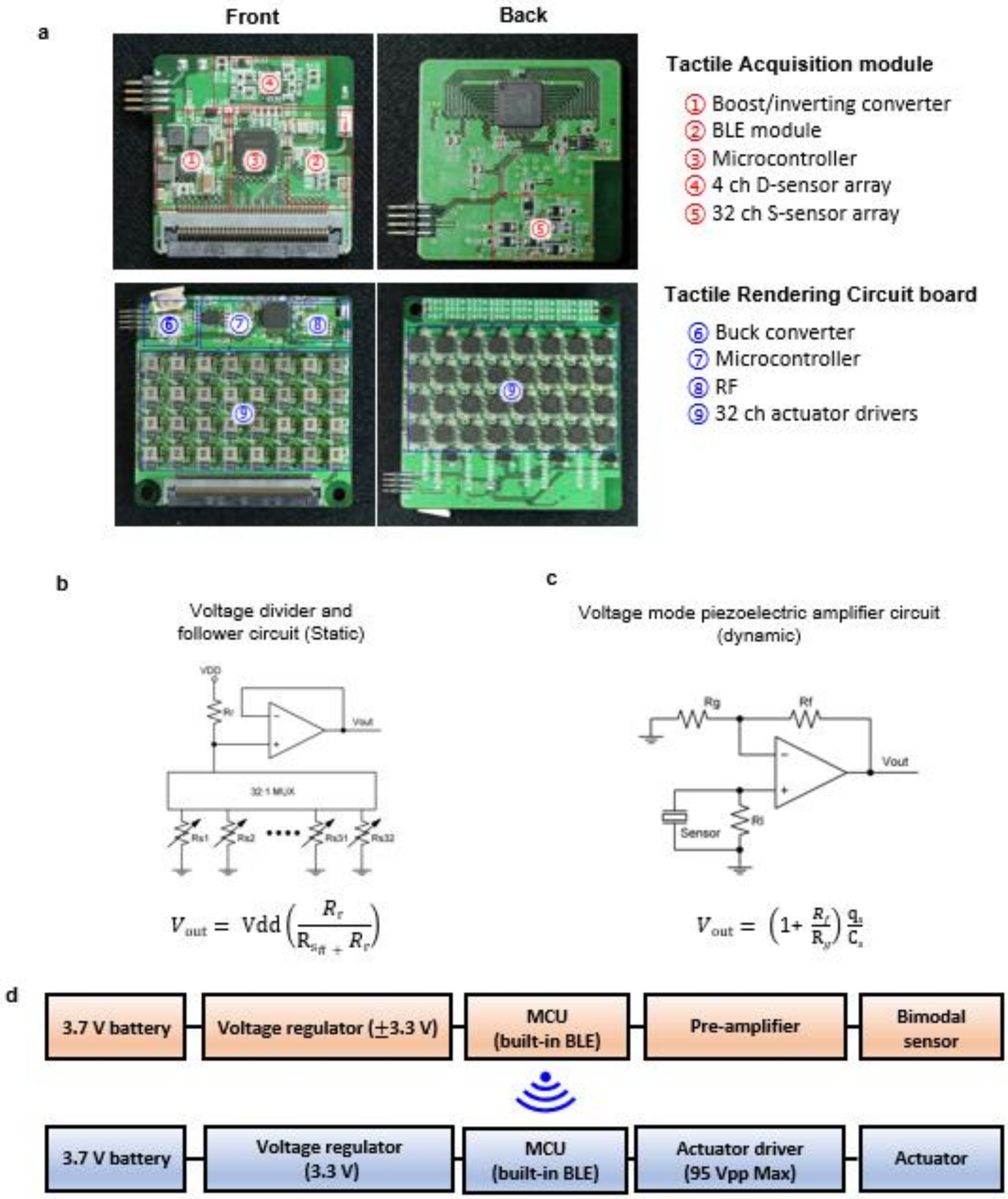

Supplementary Figure 11. Design and circuit diagram of telehaptic system. **a**, Image of wireless circuit board, **b**, circuit diagram of static pressure sensor, **c**, circuit diagram of dynamic pressure sensor, **d**, system block diagram of wireless board for telehaptic system.

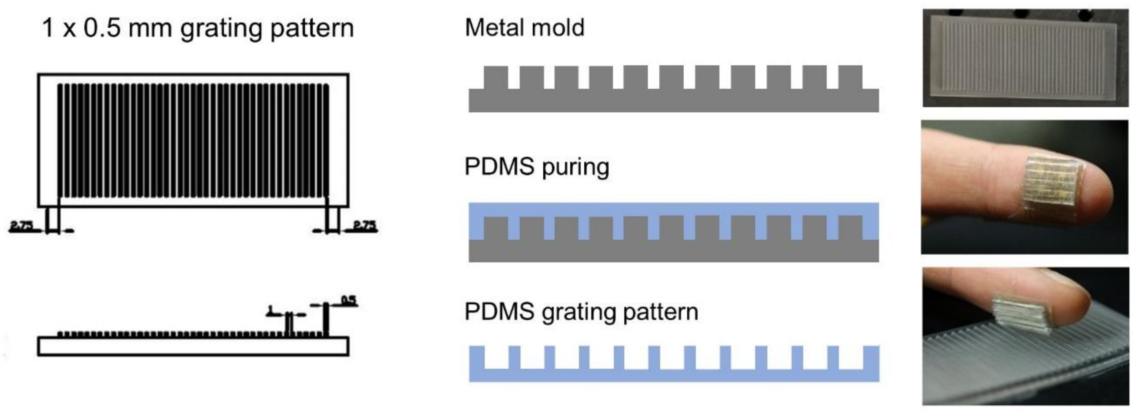

Supplementary Figure 12. PDMS grating pattern for vibration amplifier. Grating PDMS film has a width of 0.5 mm and a gap of 1 mm.

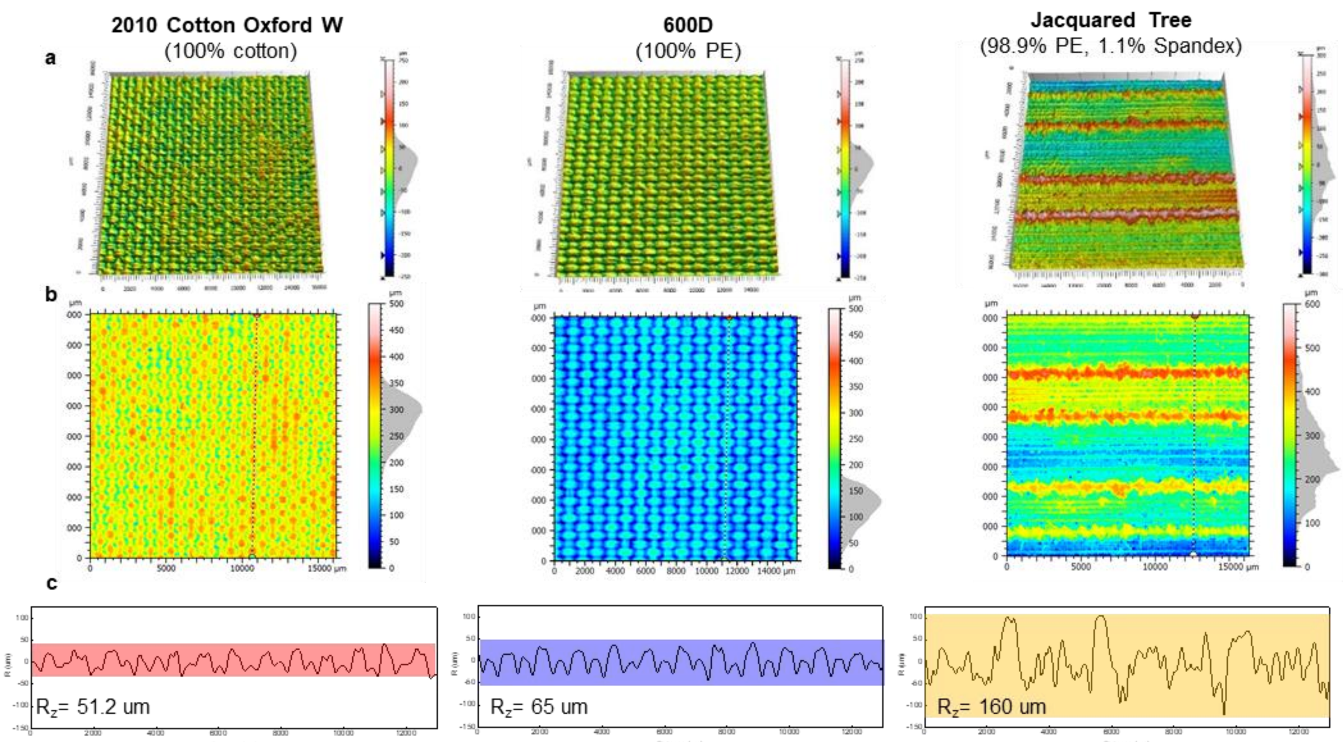

Supplementary Figure 13. Surface roughness of textile. **a**, 3D scan of 3 different types of fabric (2010 cotton oxford W, 600D, Jacquared Tree) by confocal microscopes. **b**, 2D images of each fabric. **c**, line profile is plotted to quantify the roughness of fabrics through the vertical average maximum height. R_z is a mean roughness depth.

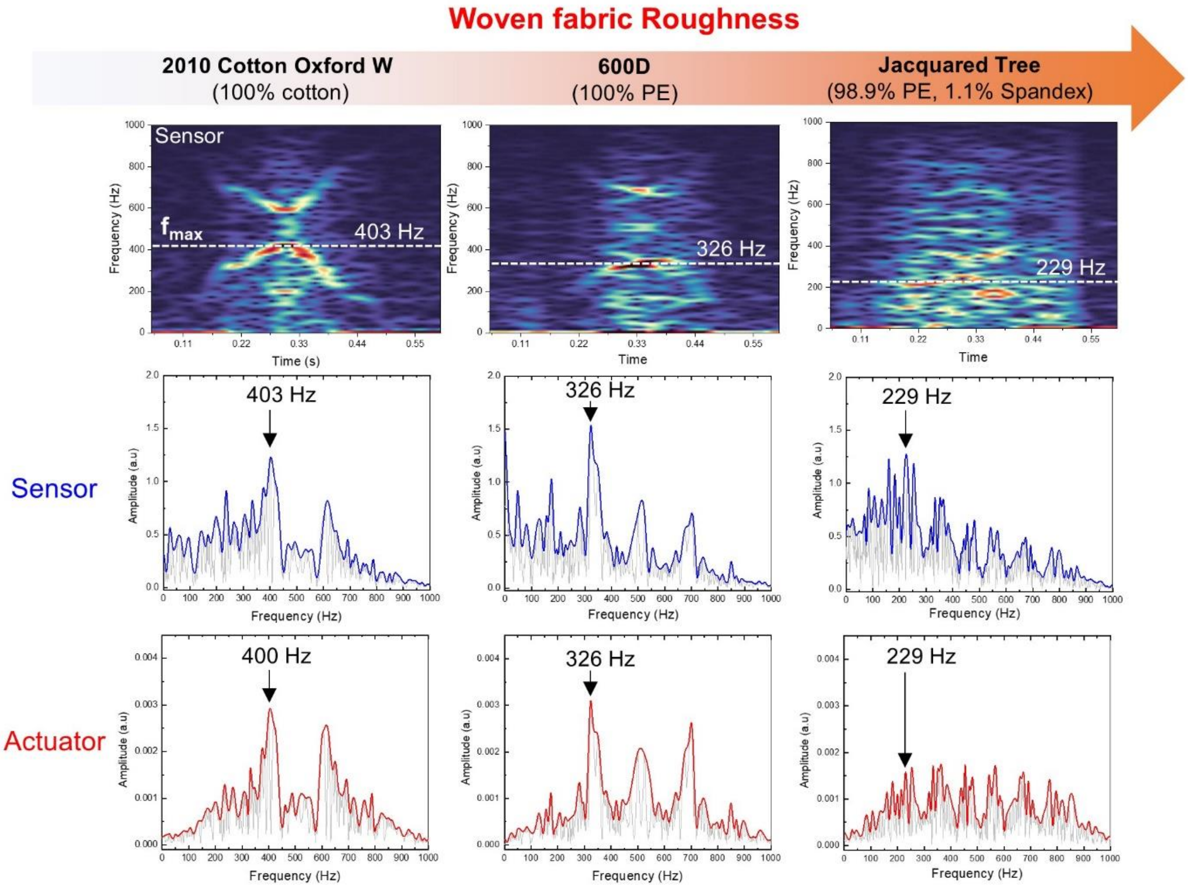

Supplementary Figure 14. Correlation of tactile acquisition and rendering system. STFT spectrogram of sensor signal corresponding to fabric 1: 2010 cotton oxford W, 100% cotton (left), fabric 2: 600D, 100% polyester (centre), and fabric 3: Jacquard Tree, 98.9% polyester, 1.1% Spandex (right). FFT spectrum of sensor signal (blue) for 3 different fabric and actuator signal (red).

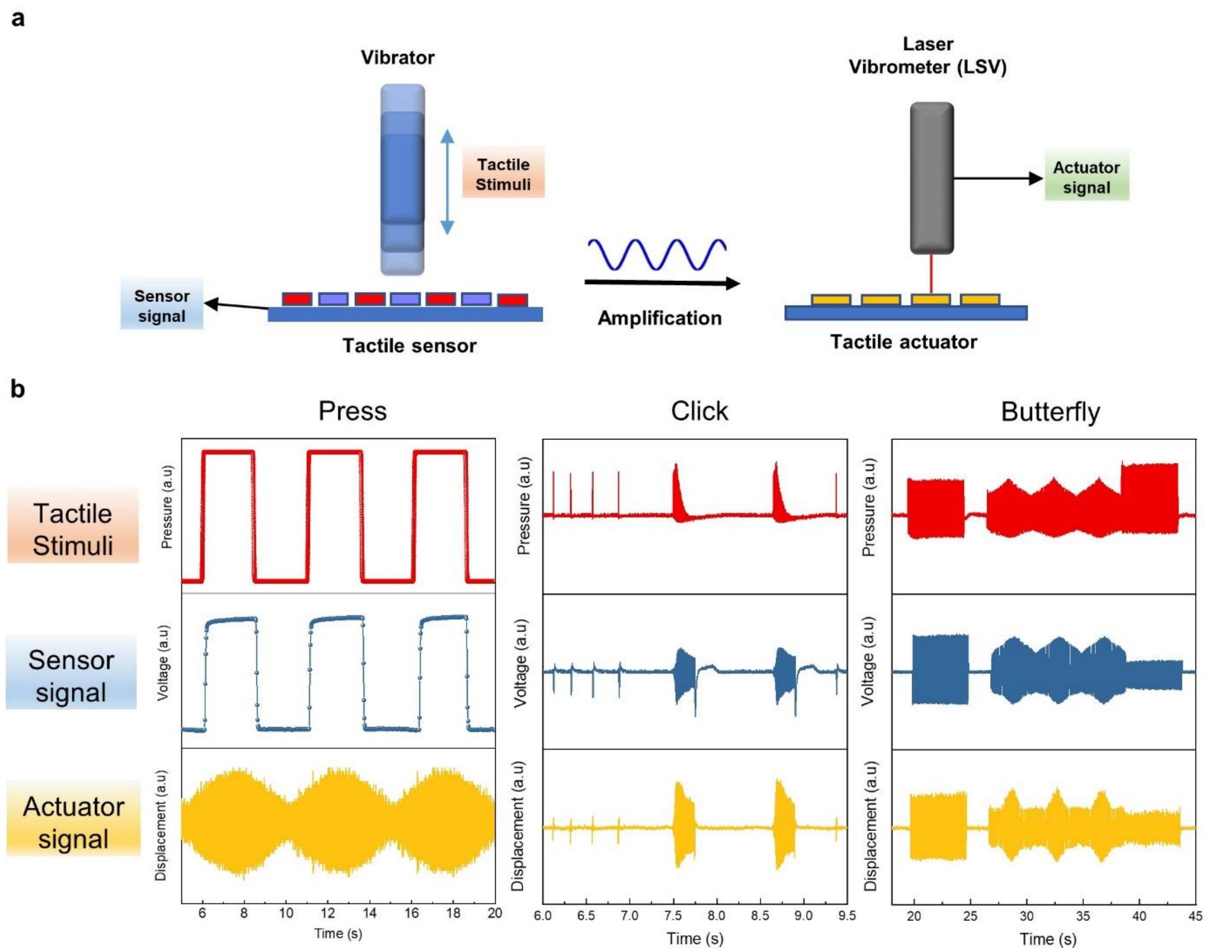

Supplementary Figure 15. Demonstration of tactile acquisition and rendering system. **a**, Schematic of tactile acquisition and rendering system. Tactile stimuli were generated by vibrator and detected by tactile sensor. Transmitted tactile signals are rendered by tactile actuator and measured by LSV equipment. **b,** tactile stimuli measured by commercial force transducer (B&K 8001), UFB tactile sensor signal, and the displacement of tactile actuator during the press, by applying click and butterfly wing flapping pattern.

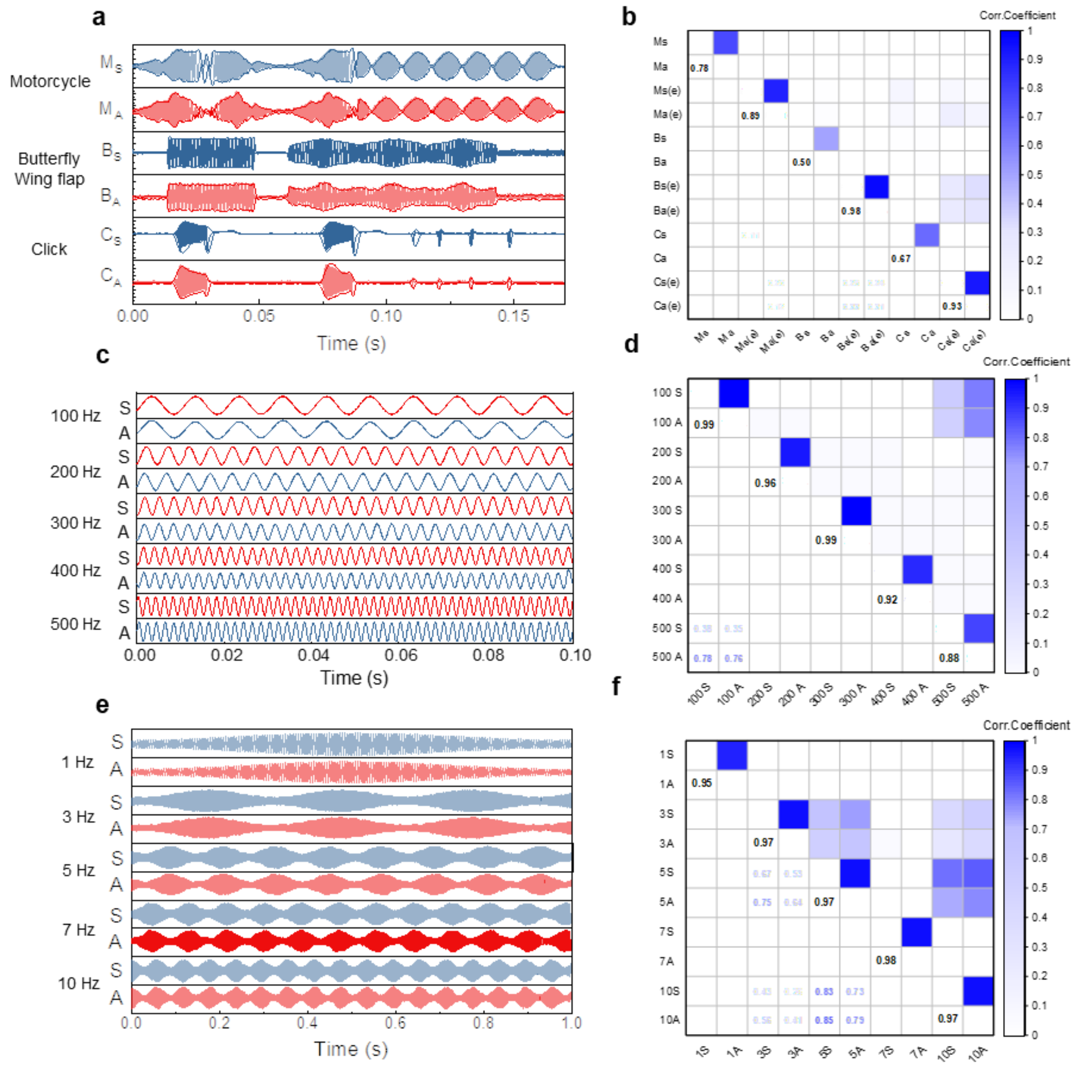

Supplementary Figure 16. Correlation of tactile acquisition and rendering system. Acquired tactile sensor output voltage(red) and rendered vibrational displacements(blue) of tactile actuator by transmitted sensor signals. The waveforms are **a,** motorcycle (M_S, M_A), butterfly flapping (B_S, B_A), and click (C_S, C_A) (boreas 1901 evaluate kit). **b,** correlation matrix correlogram between the signals acquired by the sensor (M_S, B_S, C_S) and the rendered actuator signals (M_A, B_A, C_A). The $M_{S,\ A}$(e), $B_{S,\ A}$(e) and $C_{S,\ A}$(e) were envelope of sensor and actuator signals. The waveforms of sensor and actuator **c**, at 100-500 Hz and **e**, amplitude modulation (1-10 Hz) with carrier frequency of 300 Hz. **d, f**, correlation matrix of each waveforms describing correlation coefficient between acquired sensor and rendered actuator signals.

Supplementary Table. 1. High-resolution haptic array system

Type	Resolution(pitch) /channels	Output performance (Displacement)	Response time	Flexibility (Bending radius)
Electromagnetic[1)]	2 cm / 32 ch	35 μm	2.3 ms*	Flexible (51 mm)
Hydraulically amplified electrostatic[2)]	6 mm / 25 ch	500 μm	5 ms	Flexible 112 μm PET film (Not measured)
Pneumatic/ bistable electroactive polymer[3)]	2.5 mm / 16 ch	700 μm	~1 s	Rigid Pneumatic chamber
Piezoelectric (This work)	1.8 mm / 32 ch	1 μm	1.55 ms*	Highly Flexible (3 mm)
Human finger (detection threshold)	1 mm[4)]	0.2 μm (@ 200-300 Hz)[5)]	0.385 ms[6)]	Index finger radius (7.5 mm)[7)]

Supplementary Table 2. Performance comparison of PZT actuators

Type	Dimension (volume)	Piezoelectric constant, d_{33}	Displacement	Acceleration	Mechanical features	Minimum bending radius
Conventional PZT actuator (TDK, Corp.)	9×9×0.55 mm ($44.55\ mm^3$)	-	35 μm	2.5 G	Rigid	Not bendable
Thin film sol-gel PZT[8)]	0.15×1×0.02 mm ($0.003\ mm^3$)	200	Not measured	Not measured	Flexible	0.3 mm[9)]
Micro PZT array (This work)	1×1×0.8 mm ($0.8\ mm^3$)	520 (PZT-K148)	1 μm	0.2 G	Flexible	3 mm

Supplementary Reference

1. X. Yu et al. Skin-integrated wireless haptic interfaces for virtual and augmented reality, *Nature* **575**, 473–479 (2019),
2. E. Leroy et al. Multimode Hydraulically Amplified Electrostatic Actuators for Wearable Haptics, *Adv. Mater.* **32**, 2002564, (2020)
3. Y. Qiu et al. Refreshable Tactile Display Based on a Bistable Electroactive Polymer and a Stretchable Serpentine Joule Heating Electrode, *ACS Appl. Mater. Interfaces* **10**, 24807–24815 (2018)
4. R. W. Van Boven, Tactile spatial resolution in blind Braille readers, *Neurology* **54**, 2230-2236 (2000)
5. Q. V. Duong et al. Audio-Tactile Skinny Buttons for Touch User Interfaces, *Sci. Rep.* **9**, 13290 (2019)
6. A. W. Y. Ng et al. Finger Response Times to Visual, Auditory and Tactile Modality Stimuli, *Proc. IMECS* **2**, (2012)
7. B. Hohendorff et al. Lengths, girths, and diameters of children's fingers from 3 to 10 years of age. *Ann. Anat.* **192**, 156-161 (2010)
8. V. Natarajan et al. Studies on piezo coefficients of PLD and sol-gel grown PZT thin film for devices. *Integr. Ferroelectr*. **193**, 100-105, (2018)
9. C. Dagdeviren et al. Conformal piezoelectric systems for clinical and experimental characterization of soft tissue biomechanics. *Nat. Mater*. **14**, 728–736 (2015)